Up-Grade Bypass Controlled Supercritical CO_2 Gas Turbine for 0.6 GW$_{th}$ FFHR Series Fusion Reactors*)

Sintaro ISHIYAMA, Akio SAGARA[1], Hirotaka CHIKARAISHI[1] and Nagato YANAGI[1]

School of Fundamental Science and Engineering, Waseda University,
3-4-1 Ohkubo, Shinjuku-ku, Tokyo 169-8555, Japan
[1]*National Institute for Fusion Science, 322-6 Oroshi, Toki, Gifu 509-5292, Japan*

For the purpose of further improving the power generation performance by the supercritical CO_2 gas turbine power generation system, aerodynamic optimum and heat transfer flow analysis were carried out for vertical single-axial bypass control type supercritical CO_2 gas turbine power generation system model in the 0.6 GW class FFHR-b1 nuclear fusion power reactor model. As a result, the following conclusions were obtained.

(1) Since the outlet temperature of the 5-stage final stage of the improved main compressor as an alternative to the low/high pressure compressor can be lowered to 318 K compared to the conventional design (outlet temperature 334 K), there are design cases that do not require an intercooler in the conventional design.

(2) As a result of reviewing the structural design and operating conditions of the turbine, the output increased by about 1.1%.

(3) Since a compact design with a total length of about 2.2 m is possible in the design of the above CO_2 gas turbine power generation system (excluding the generator), the feasibility of designing a vertical single-axial bypass control type supercritical CO_2 gas turbine power generation system is clarified.

From these results, the redesigned vertical uniaxial bypass control type supercritical CO_2 gas turbine power generation system is expected to be a compact and economical power generation system that exceeds the power generation efficiency of the conventional design model up to about 0.6%.

1. Introduction

Figure 1 shows the basic configuration of the FFHR fusion reactor [1–5]. In this power generation reactor, the reaction heat generated during the fusion reaction from the FFHR is transferred to the outside of the reactor via the primary power pump type intermediate heat exchanger (IHX) through the in-core blanket and diverter through a circulating heat medium such as molten salt. Heat is transferred to the secondary power generation system of the supercritical CO_2 gas turbine power generation system [6–18].

However, in the conventional vertical single-axis design [4,5] for the secondary power generation system of the 3 GW class nuclear fusion reactor FFHR, an intercooler installed between the low (LPC)/high pressure compressors (HPC), reduces the thermal efficiency of the power generation system and increase in the vertical layout and the manufacturing cost of the secondary power generation system.

In the conventional [4–6] bypass control type supercritical CO_2 gas turbine, this intercooler prevent the in-
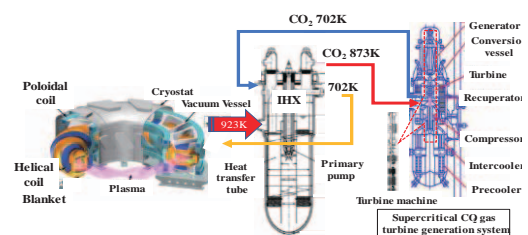

Fig. 1 Conceptual design of 3 GWth FFHT power generator system.

crease in compression power due to the high temperature of the working fluid generated when LPC is restored. However, it is expected that the temperature rise of the working fluid in the compressor can be prevented by installing a Diffuser Passage (DP) [19] on the outlet side of the compressor, and reducing the height of the moving blades and the casing volume of each stage of the compressor.

Therefore, in this paper, a scale-down model of 3 GW class FFHR [4, 5] with a heat output of 0.6 GW class nuclear fusion reactor FFHR-b1 ((Blanket/Divertor 522 MW/79 MW) operating temperature 873/703.8 K) [20–22] is used as an analysis model case, Aerodynam-

ics and structural design were carried out to improve the performance of main compressors, bypass compressors and turbines, and their performance was evaluated by heat transfer flow analysis using supercritical CO_2 actual gas data.

2. Procedures

Here, the heat transfer flow analysis by CFD (Computational Fluid Dynamics) of the aerodynamically designed bypass control type supercritical CO_2 gas turbine connected to the 0.6 GW FFHT-b1 reactor is performed.

2.1 Aerodynamic compressible fluid model

The main components of the secondary supercritical CO_2 gas turbine power generation system dealt with in this paper consist of the main compressor, bypass compressor, turbine and various heat exchangers, and the aerodynamic design targets in this paper are the main compressor, bypass compression and turbines, and heat transfer flow analysis was carried out for these constituent equipment.

The aerodynamic design of the main compressor, bypass compressor and turbine were carried out using the SCCOT design code [4, 5] based on supercritical CO_2 actual gas data. In addition, the SCCOT code designed for the heat transfer flow analysis of these aerodynamically designed high-speed rotating devices was carried out by linking with NIST actual gas data [23] using the general-purpose heat transfer flow analysis software Fluent ver. 18.

2.2 Thermodynamic and aerodynamic design criteria for compressors

The aerodynamic design of the main compressor and bypass compressor by SCCOT was carried out by setting the following five design criteria.

① De Haller number (> 0.72)

The de Haller number characterizes the amount of diffusion over the blade and is given as; V2/V1 ≥ 0.72 (2.2) where, V2 and V1 are the velocities at the trailing and leading edge respectively. The de Haller number is important to control the whirl velocity because a high whirl velocity implies a high fluid deflection and diffusion rate [24].

② Diffusion factor (< 0.5)

Decision is taken regarding the blade chord and the number of blades. Increasing the chord reduces the aspect ratio and increases solidity for the same annulus and number of blades [25]. There is need to also understand that the choice of stage loading, which has direct proportionality with the pressure rise in relation to the 16 stages and the rotational speed must be given proper considerations for a successful aerodynamic design [25].

③ Reynolds number (> 2.5E5)

The Reynolds number is one of characteristic numbers used for predicting whether a flow condition will be laminar or turbulent. It is defined as the ratio of inertial forces to viscous forces [26].

④ Blade stress (< 800 MPa)

⑤ Flow coefficient (~0.5) and pressure coefficient (~0.36)

The flow coefficient of a device is a relative measure of its efficiency at allowing fluid flow. It describes the relationship between the pressure drop across an orifice valve or other assembly and the corresponding flow rate [27]. The pressure coefficient is a dimensionless number which describes the relative pressures throughout a flow field in fluid dynamics. The pressure coefficient used in aerodynamics and hydrodynamics.

3. Results
3.1 Basic component design specification

(1) Design specification of main compressor

From the results of the optimum control shaft rotation speed dependence in the uniaxial design of low- and high-pressure compressors/turbines/generators according to the heat source scale in the previous report [4, 5], The rotation speed of the optimum rotation shaft at the 0.6 GW class FFHR-b1 heat source scale was set to 6,000 rpm, and the number of composite stages of the main compressor and the axial flow velocity of the supercritical CO_2 in the compressor were optimized.

Figures 2 (a) and (b) show the aerodynamic design results of the main compressor based on the above SCCOT code in the 0.6 GW class FFHR-b1 model. Figure 2 (a) shows the relationship between the heat duty and the main compressor adiabatic efficiency with respect to the number of stages of the main compressor, and Fig. 2 (b) shows the heat duty of main compressor and generation efficiency of the generation system with respect to the supercritical CO_2 axial flow velocity. According to this, as the number of main compressor stages and the heat duty increases, whereas the adiabatic efficiency decreases. Therefore, the optimum number of stages is set to 5 (star point in Fig. 2 (a)).

On the other hand, Fig. 2 (b) shows the star marks on the relationship curve between the axial flow velocity/heat duty and efficiency. The point indicated by this star is used as the design point because the heat duty is the minimum
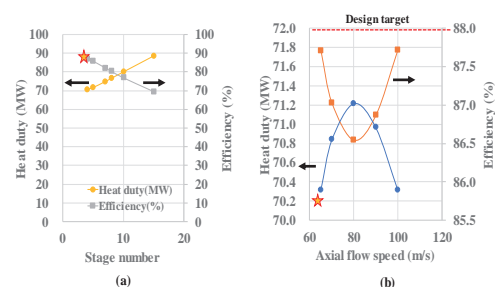

Fig. 2 Design specification of main compressor: Relationship between (a) heat duty/efficiency and stage number, (b) and axial flow speed.
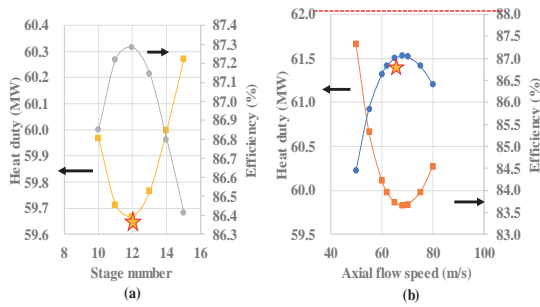
Fig. 3 Design specification of bypass compressor: Relationship between (a) heat duty/efficiency and stage number, (b) and axial flow speed.
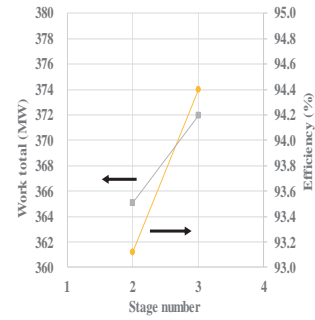

Fig. 4 Design specification of bypass compressor: Relationship between heat duty/efficiency and stage number.
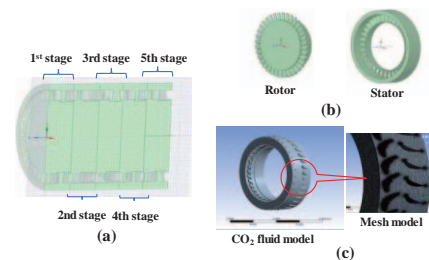

Fig. 5 Heat transfer structure analysis model of main compressor: (a) main compressor full model, (b) stage structure, (c) mesh model of CO_2 fluid model.
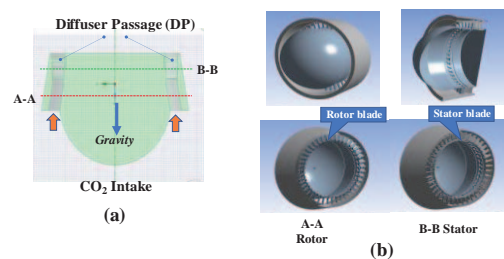

Fig. 6 Structural design model of 1st stage of main compressor.

and the adiabatic efficiency is the maximum. Based on the above results, the basic design specifications of the main compressor are shown below.

　　Operation In/Outlet temperature : 328.5/308 K

　　In/Outlet pressure : 35.72/9.33 MPa

　　CO2 mass flow rate : 2824.525 kg/s

　　Stage number : 5

　　Rotation speed : 6000 rpm

　　Axial flow speed : 65 m/s

　　Heat duty : 71.8 MW

　　(2) Design specification of bypass compressor

　　Similar to the main compressor specifications, the higher performance designed point of the bypass compressor is indicated by the stars in the figure in Figs. 3 (a) and (b). From this result, 12 stages with the minimum heat duty were set as the optimum number of composite stages, and the axial flow speed in Fig. 3 (b) was set to 63 m/s.

　　Based on the above results, the basic design specifications of the bypass compressor are shown below.

　　Operation In/Outlet temperature : 341/341 K

　　In/Outlet pressure : 9.42/9.42 MPa

　　CO_2 mass flow rate : 1037.33 kg/s

　　Stage number : 12

　　Rotation speed : 6000 rpm

　　Axial flow speed : 63 m/s

　　Heat duty : 60 MW

　　(3) Design specification of turbine

　　Figure 4 shows the relationship between the number of turbine stages and work and adiabatic efficiency. According to this, it is possible to obtain a maximum work of 374 MW and adiabatic efficiency of 94.2% with 3-stages. Based on these facts, the turbine design specifications are shown below.

　　Operation In/Outlet temperature : 873.2/758.6 K

　　In/Outlet pressure : 25/9.62 MPa

　　CO_2 mass flow rate : 2824.53 kg/s

　　Stage number : 3

　　Rotation speed : 6000 rpm

　　Adiabatic efficiency : 94.2%

　　Total work : 374 MW

3.2　Heat transfer structure analysis model and component performance

　　Here, the results of heat transfer flow analysis using CO_2 fluid model of a 5-stage main compressor, a 12-stage bypass compressor, and a 3-stage turbine according to the basic design specifications in 3. Results 3.1 (1) above are shown.

　　Figure 5 shows the compressor full model (a), its 1st-stage model configuration (b), and the CO_2 fluid model (c) for heat transfer structure analysis.

　　The compressor model consists of rotor, stator and a CO_2 fluid model that flows in these structures. In the heat transfer fluid analysis, the rotor part in this CO_2 fluid model was rotated at a predetermined rotation speed (6000 rpm) to analyze the flow status of the CO_2 fluid in the structure.

　　(1)　Main compressor

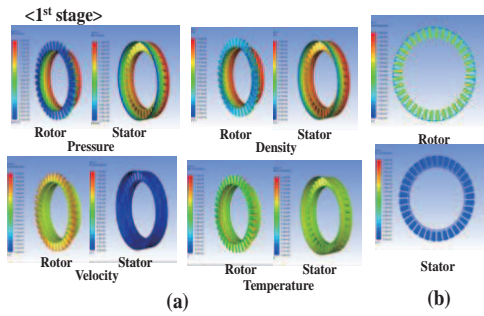　　Figure 6 shows the CO_2 fluid passage (a) and struc-

Fig. 7 The flow status of the CO_2 fluid in the 1st stage of main compressor: (a) status distribution and (b) velocity vector distribution.
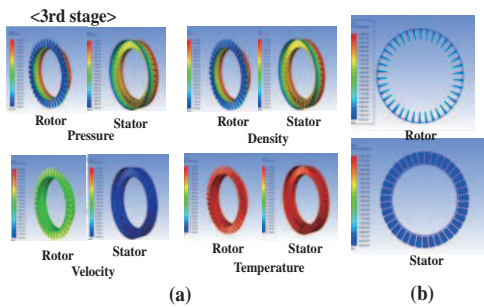

Fig. 8 The flow status of the CO_2 fluid in the 3rd stage of main compressor: (a) status distribution and (b) velocity vector distribution.
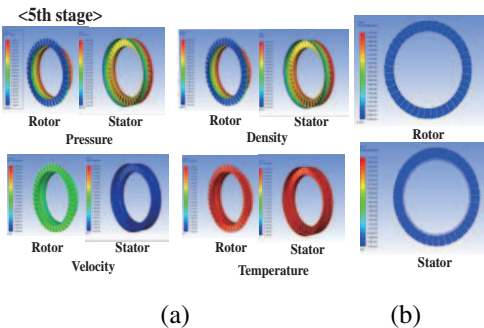

Fig. 9 The flow status of the CO_2 fluid in the 5th stage of main compressor: (a) status distribution and (b) velocity vector distribution.

tural model (b) of the 1st stage of the main compressor. As shown in Fig. 6 (a), the CO_2 fluid in this design flows in from the vertically arranged compressor rotor part against the gravity.

Figures 7 to 9 show changes in the pressure, density, velocity, and temperature of CO_2 flowing into the1st, 3rd, and final stages (3rd stage) of the main compressor (a), and the velocity vector of the CO_2 fluid flowing on the surface of each blade of the rotor and stator (b), respectively.

It can be seen that the degree of change in the physical property values increases as the change in each physical property value on the constituent devices in the figure
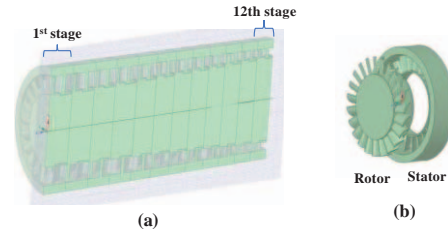

Fig. 10 Heat transfer structure analysis model of main compressor: (a) main compressor full model, (b) stage structure.
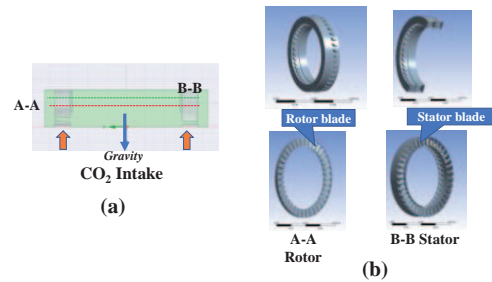

Fig. 11 Heat transfer structure analysis model of bypass compressor: (a) CO2 channel model and (b) CO_2 fluid model.

changes from blue to red.

From the results of various state distributions in each stage, it was not possible to confirm the existence of discontinuous singular points such as stagnation and separation points of the CO_2 fluid in each part of the rotor and stator that adversely affect the compressor performance.

In the velocity vector change on the surface of each rotor blade, a high-speed flow velocity region exists locally in the center of the 1st-stage rotor blade, and this high-speed flow velocity region moves to the blade tip in the 3rd-stage rotor blade. On the other hand, on the surface of the final stage rotor blade, it can be seen that these high-speed basins have been eliminated and the velocity of the entire blade surface has been made uniform.

(2) Bypass compressor

Figure 10 shows the overall model structure (a) of the 12-stage bypass compressor and the basic structure (b) of each stage. The basic structure is a combination of rotor and stator.

Figure 11 shows the CO_2 flow channel path (a) in the 1st stage and the CO_2 fluid model structure (b) for heat transfer structure analysis.

Figures 12 to 14 show changes in the pressure, density, velocity, and temperature of CO_2 flowing into the 1st, 6th, and final stages (12th stage) of the bypass compressor (a), and the velocity vector of the CO_2 fluid flowing on the surface of each blade of the rotor and stator (b), respectively.

Comparing the above-mentioned main compressor configurations, it can be seen that the blade width and length are increasing, although the number of blades in
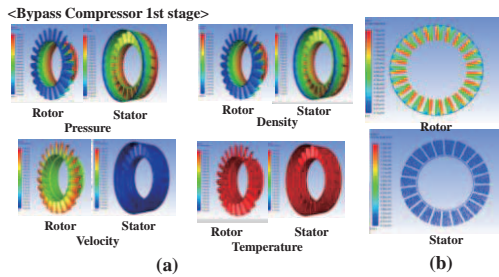
Fig. 12 The flow status of the CO_2 fluid in the 1st stage of bypass compressor: (a) status distribution and (b) velocity vector distribution.
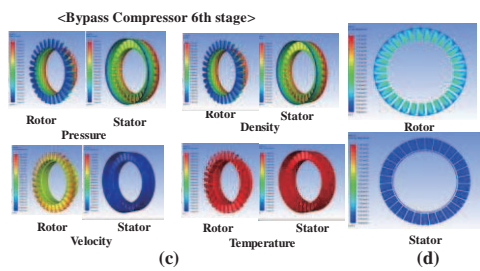

Fig. 13 The flow status of the CO_2 fluid in the 6th stage of bypass compressor: (a) status distribution and (b) velocity vector distribution.
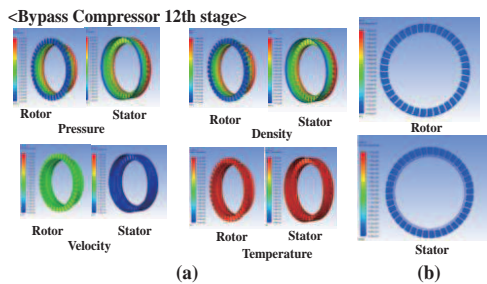

Fig. 14 The flow status of the CO_2 fluid in the 12th stage of bypass compressor: (a) status distribution and (b) velocity vector distribution.

each stage of the bypass compressor is decreasing.

From the results of various state distributions in each stage, the existence of discontinuous singular points such as the stagnation point of the CO_2 fluid in each part of the rotor and stator, which adversely affects the compressor performance, could not be confirmed in the bypass compressor.

On the other hand, in the velocity vector change on the surface of each rotor and stator blade, unlike the main compressor, the high-speed flow velocity region is concentrated at the tip of the 1st-stage rotor blade.

In this high-velocity flow portion, the velocity uniformization is progressing in the entire 6th stage rotor blade, and these high-velocity basins are eliminated in the final stage rotor blade surface, and the velocity uniformization is progressing in the entire blade surface.
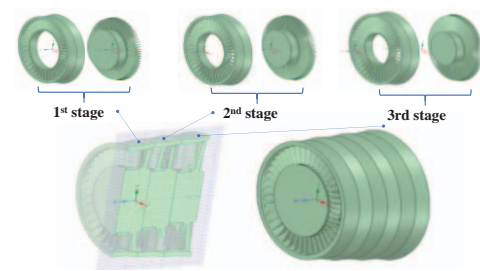

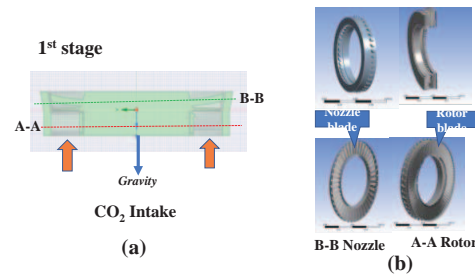Fig. 15 Heat transfer structure analysis model of turbine.

Fig. 16 Heat transfer structure analysis model of turbine: (a) CO_2 channel model and (b) CO_2 fluid model.
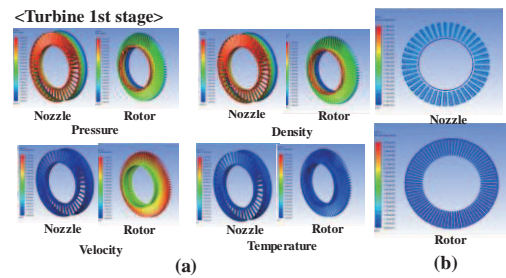

Fig. 17 The flow status of the CO_2 fluid in the 1st stage of turbine: (a) status distribution and (b) velocity vector distribution.
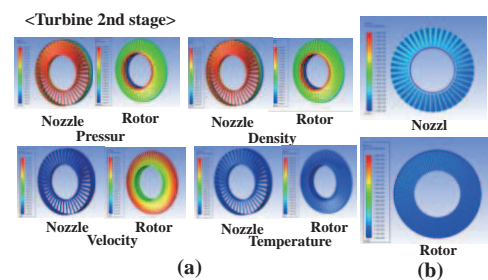

Fig. 18 The flow status of the CO_2 fluid in the 2nd stage of turbine: (a) status distribution and (b) velocity vector distribution.

(3) Turbine

Figures 15 and 16 show the overall model structure of the turbine with a three-stage configuration, the CO_2 channel flow path (a) in a single stage, and the CO_2 fluid model (b) for heat transfer structure analysis. Each stage of the turbine consists of a nozzle and rotor combination.
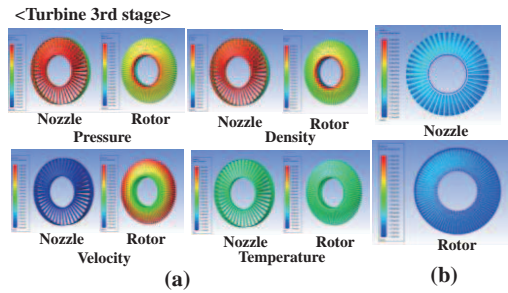
Fig. 19 The flow status of the CO_2 fluid in the 3rd stage of turbine: (a) status distribution and (b) velocity vector distribution.
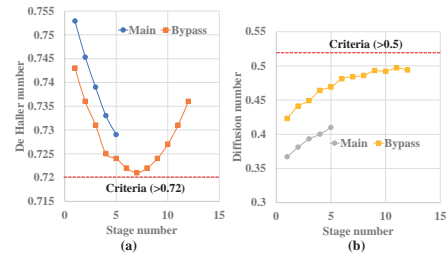

Fig. 20 The flow status of the CO_2 fluid in main and bypass compressor with its design criteria: (a) de Haller number and (b) diffusion factor.
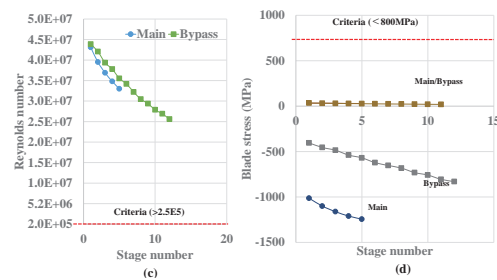

Fig. 20 The flow status of the CO_2 fluid in main and bypass compressor with its design criteria: (c) reynolds number and (d) blade stress.
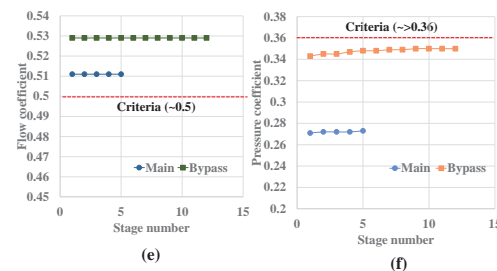

Fig. 20 The flow status of the CO_2 fluid in main and bypass compressor with its design criteria: (e) flow coefficient and (f) pressure coefficient.

Figures 17 to 19 show the changes in the pressure, density, velocity, and temperature of CO_2 flowing into the 1st, 2nd, and final stages of the turbine (a), and the velocity vector distribution of the CO_2 fluid flowing on the surface of each blade of the nozzle and rotor (b) is shown, respectively.

Unlike the compressor described above, the high-temperature and high-pressure CO_2 fluid flowing into the turbine collides with the tip of the non-rotating nozzle blade at each stage at high speed, while velocity of CO_2 fluid on the surface of the rotating rotor blade is distributed almost uniformly.

4. Discussion

4.1 Rotor-dynamic Analysis and stress calculation

4.1.1 Model check on CO_2 fluid flow in compressors

Here, the feasibility of the CO_2 flow state in the compressor obtained by CFD was verified by comparing it with the various criteria set in (2.2).

Figures 20 (a) to (f) show a comparison between the de Haller number, Diffusion factor, Reynolds number, Blade stress, Flow and pressure coefficient values and various criteria levels in each compressor configuration stage. The de Haller number values in each stage of the main and bypass compressors change according to the velocity change (Figs. 21 (a) (b)) of each stage, which will be described later and these values clear the design setting criteria (> 0.72) in all stages (Fig. 20 (a)). The Reynolds number values at each stage of both compressors also clear the criteria (> 2.5E5) (Fig. 20 (b)). The bending stress and compressive stress level (Fig. 20 (c)) generated in the blade stress of each stage are all below the criterion value (< 800 MPa). The flow and pressure coefficient values in each stage almost clear the criteria conditions.

As a result of the above, all the criteria given were cleared in the main compressor and the bypass compressor.

4.1.2 Physical continuity [28]

In order to check the presence of local fluid separation and singularity that occur in the high-speed rotating

equipment model, it is necessary to accurately know the flow state of the supercritical CO_2 fluid in the compressors. For that purpose, it is important to know the physical flow change of CO_2 in the supercritical state in the compressors [4, 5].

Figures 21 (a)~(f) and Figs. 21 (g)~(k) show the change in various physical property of supercritical CO_2 fluid at the inlet and outlet of each stage of the main compressor, bypass compressor and turbine.

Figures 21 (a)~(b) show the temperature/pressure and density changes at each stage in the main and bypass compressors, respectively.

According to this, it can be seen that the supercritical density also continuously increases from 600 MPa to 850 MPa in response to the temperature and sudden pressure change (a) that occur at the inlet and outlet of the main
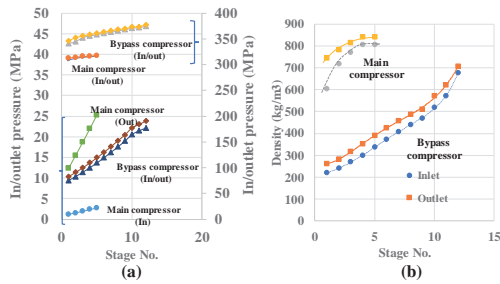
Fig. 21 The flow status of the CO_2 fluid in main and bypass compressor: Change in (a) temperature/pressure and (b) density.
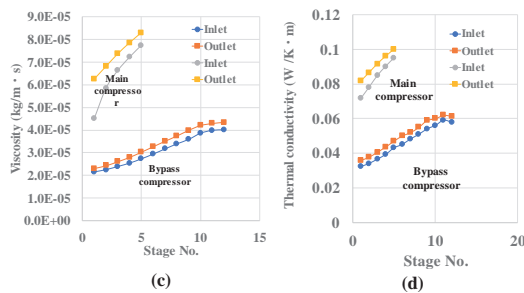

Fig. 21 The flow status of the CO_2 fluid in main and bypass compressor: Change in (c) viscosity and (d) thermal conductivity.
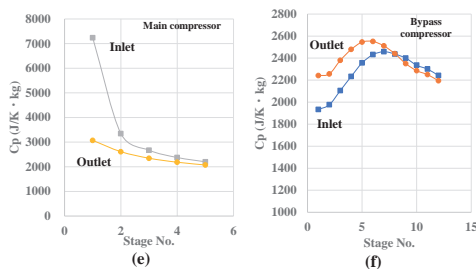

Fig. 21 The flow status of the CO_2 fluid in main and bypass compressor: Change in Cp of (e) main and (f) bypass compressor.
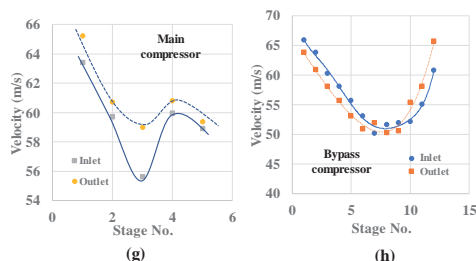

Fig. 21 The flow status of the CO_2 fluid in main and bypass compressor: Change in velocity of (g) main and (h) bypass compressor.

compressor.

In the bypass compressor, a rapid density change (Fig. 21 (b)) occurs continuously and gradually from about 200 MPa to 700 MPa in the process of increasing the pressure.

Figures 21 (c)~(d) show changes in viscosity and thermal conductivity at each stage of the main and bypass compressors. Both show a monotonically increasing tendency according to the temperature and pressure change in Fig. 21 (a).

Figures 21 (e)~(f) show the changes in the specific heat C_p at each stage of the main and bypass compressors. According to this, in the main compressor, C_p decreases as the pressure increases, and it tends to decrease sharply especially at the entrance from the 1st stage to the 2nd stage (Fig. 21 (e)).

In the conventional design model [4, 5], the temperature rise of the CO_2 working fluid in the supercritical state in the low-pressure compressor is considered to be due to this phenomenon.

On the other hand, the C_p value of low-density CO_2 in the bypass compressor tends to increase, indicating that the temperature rise of the working CO_2 fluid in each stage is not as high as that of the main compressor.

Figures 21 (g)~(h) show the changes in the flow velocity of the supercritical CO_2 fluid in each stage of the main compressor and bypass compressor, respectively.

In the main compressor, the speed continued to decrease from the first stage to the third stage, but the speed tended to recover after the third stage. This similar tendency was also observed in the 8th and subsequent stages of the bypass compressor [28].

Figures 22 (a)~22 (b) show the changes in temperature, pressure and flow velocity at the inlet and outlet of each stage of the turbine. From this result, it can be seen that a rapid decrease in temperature and pressure occurs at each stage in the turbine. On the other hand, it can be seen that the CO_2 fluid velocity in the supercritical state in the turbine is about 100 m/s, which is a high-speed fluid state with respect to the above-mentioned compressor (~60 m/s).

Figures 22 (c)~(f) show the density, viscosity, thermal conductivity, and specific heat change in the turbine, respectively. These physical properties decreased monotonically according to the decreasing tendency of the density in each stage of the turbine in Fig. 22 (c).

From the results of these changes in physical properties at each stage, it was not confirmed the existence of discontinuities such as local fluid separation and singularities in the flow state of CO_2 fluid in each component.

4.2   Improvement for high performance of turbine design

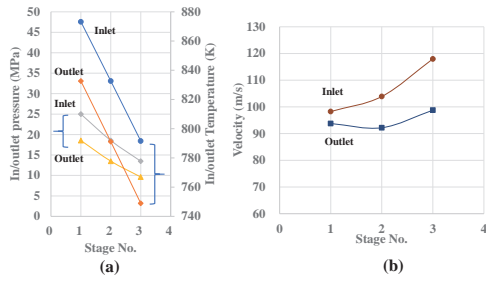Here, the initial design of the main and bypass compressors and the turbine model of the supercritical CO_2 gas

Fig. 22 The flow status of the CO_2 fluid in turbine: Change in (a) pressure/temperature and (b) velocity.

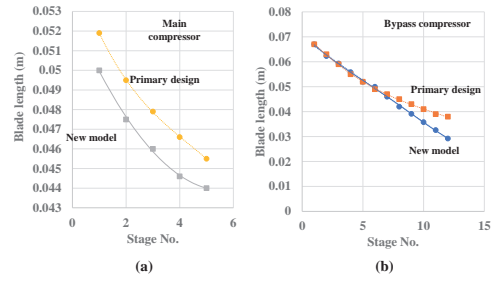
Fig. 23 Model change in main and bypass compressor: change in blade height of (a) main and (b) bypass compressor.
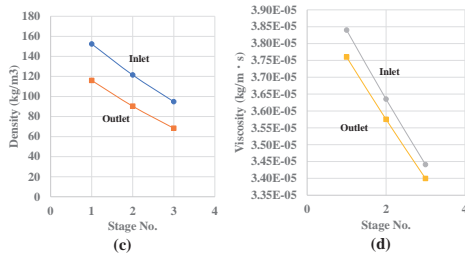

Fig. 22 The flow status of the CO_2 fluid in turbine: Change in velocity of (c) density and (d) viscosity.
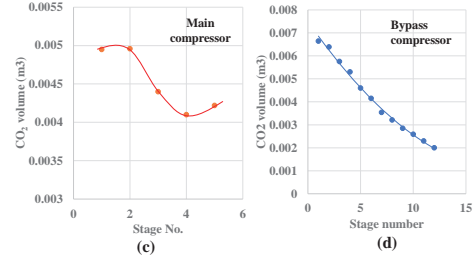

Fig. 23 Model change in main and bypass compressor: change in CO_2 volume of (c) main and (d) bypass compressor.
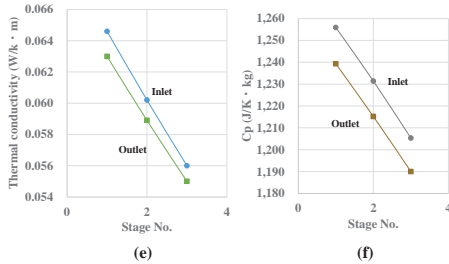

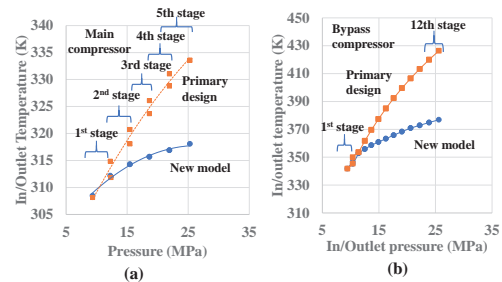Fig. 22 The flow status of the CO_2 fluid in turbine: Change in thermal (e) conductivity and (f) heat capacity.

Fig. 24 Model change in main and bypass compressor: Change in In/out temperature of (a) main and (b) bypass compressor.

turbine power generation system [4, 5] were improved in order to solve the various problems described in Chapter 1.

The main design change is the elimination of the high compressor outlet temperature. There are two design changes for that purpose. First, the Diffuser Passage (DP) structure [19] shown in Fig. 6 (a) is provided at the outlet of each stage of the main and bypass compressors. Next, in order to increase the pressure ratio of compressible supercritical CO_2 in the compressor, the height of each stage blade is shortened as shown in Figs. 23 (a) (b) and the volume inside the compressor is reduced as shown in Figs. 23 (c) (d).

The outlet temperature after the design change are shown in Figs. 24 (a) and (b) in comparison with the conventional design. According to this, the outlet temperature after the design change in the main compressor was lowered to 318 K, which is about 20 K lower than the initial value (334 K).

Furthermore, in the bypass compressor, the temperature was lowered to 380 K, which is about 40 K lower than the initial value (412.8 K).

This design change eliminates the exhaust heat (corresponding to about −16% of the total power output) from the intercooler between the low and high compressors in the conventional design [4], and improves the compression rate in the lower temperature of the bypass compressor that works in lower temperature than the main compressor. As a result, heat duty of the bypass compressor could be reduced (about −4%).

On the other hand, in the turbine, the blade height as shown in Fig. 25 (a) was changed to be slightly longer, but the CO_2 volume as shown in Fig. 25 (b) was not significantly redesigned to avoid the increase in size of the power generation system.
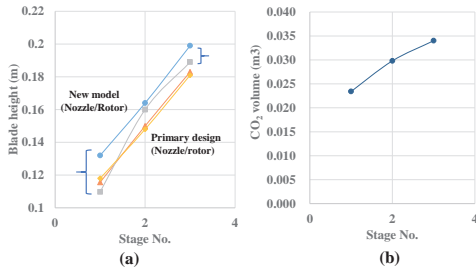
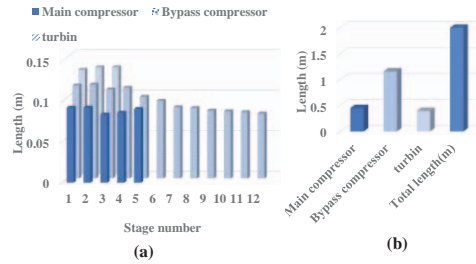Fig. 25 Model change in turbine: Change in (a) blade height and (b) CO_2 volume.

Fig. 26 0.6 GW FFHR-b1 power plant model and its heat and mass balance.

Fig. 27 Total length of supercritical CO_2 gas turbine components.
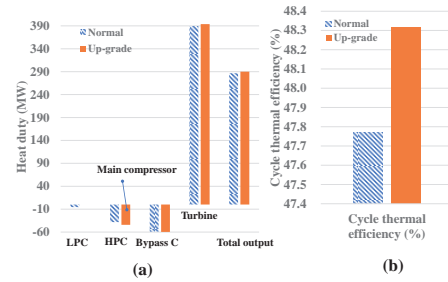

Fig. 28 Performance of up-grade 0.6 GW FFHR-b1 power plant model: Comparison between normal and up-grade design of (a) heat duty on components and (b) cycle thermal efficiency.

4.3 Up-grade FFHR-b1 power generation system

4.3.1 Component compactness

Figure 26 shows the 0.6 GW class FFHR-b1 power plant configuration redesigned in this paper and the heat mass balance in the system. In the previous report, the 3 GW class FFHR power generation system had two supercritical CO_2 power generation systems installed side by side [4, 5], but with this power generation system, 48.3% of the total heat output can be converted to electrical output.

Figures 27 (a) and (b) show the individual stage length (a) of each component, the length of each component, and the total length of the supercritical CO_2 gas turbine power generation system (excluding the generator) (b), respectively.

As a result, the total length of the power generation system is about 2.2 m (main compressor total length: 0.45 m, bypass compressor total length: 1.32 m, turbine total length: 0.39 m), which is an extremely short body. From this, the installation method of this power generation system can be installed vertically as shown in Fig. 1.

4.3.2 Performance improvement

Figures 28 (a) and (b) show the results of comparing the power generation performance of the improved design model of this power generation system with that of the conventional type.

As a result of replacing the LPC/HPC with the main compressor in this improved model (Fig. 28 (a)), the heat duty of the main and bypass compressors is slightly higher, while the improved model turbine is about 1.1%

(4.24 MW).

The overall output of the power generation system can be improved by replacing with the main compressor and eliminating the intercooler equipment. From these results of the thermal cycle efficiency as shown in Fig. 28 (b), it is expected that the thermal efficiency will be improved by about 0.6% compared to the conventional type.

5. Conclusion

For the purpose of realizing high-efficiency power generation by the thermal output 0.6 GW class nuclear fusion reactor FFHR-b1 (Blanket/Divertor 522 MW/79 MW, operating temperature 873/703.8 K), the optimization and rationalization design change of the main components in the bypass controlled supercritical CO_2 gas turbine power generation system were implemented with real supercritical CO_2 gas data, and the following results were obtained.

(1) The outlet temperature of the improved main compressor as an alternative to the low/high pressure compressor can be lowered to 318 K compared to the conventional design (outlet temperature 334 K), which simplifies the need for an intercooler. The feasibility of designing a vertical bypass control type supercritical CO_2 gas turbine power generation system was clarified.

(2) As a result of reviewing the structural design and operating conditions of the turbine, the output increased by about 1.1%.

(3) The supercritical CO_2 gas turbine power generation system (excluding the generator) is designed to be

compact with a total length of only 2.2 m and based on the result of (1) above, a simplified vertical arrangement is possible.

The bypass-controlled supercritical CO_2 gas turbine power generation system redesigned based on the above redesign results are expected to be compact and improve power generation efficiency up to about 0.6%.

Acknowledgments

[1] A. Sagara, H. Tamura, T. Tanaka, N. Yanagi, J. Miyazawa, T. Goto, R. Sakamoto, J. Yagi, T. Watanabe, S. Takayama and the FFHR Design Group, Helical Reactor Design FFHR-d1 and c1 for Steady-state DEMO, Fusion Eng. Des. **89**, 2114 (2014).

[2] A. Sagara, J. Miyazawa, H. Tamura, T. Tanaka, T. Goto, N. Yanagi, R. Sakamoto, S. Masuzaki, H. Ohtani and The FFHR Design Group, Two conceptual designs of helical fusion reactor FFHRd1A based on ITER technologies and challenging ideas, Nucl. Fusion **57**, 086046 (2017).

[3] A. Sagara, T. Tanaka, J. Yagi, M. Takahashi, K. Miura, T. Yokomine, S. Fukada and S. Ishiyama, Fusion Sci. Technol. **68**, 303 (2015).

[4] S. Ishiyama, H. Chikaraishi and A. Sagara, Operating scenario of 3 GWth class FFHR power plant with bypass controlled supercritical CO_2 gas turbine power generation system, Fusion Eng. Des. **164**, 112194 (2021).

[5] S. Ishiyama, H. Chikaraishi and A. Sagara, Aerodynamic design of Bypass controlled supercritical CO_2 gas turbine full scale model for 3 GWth FFHR, Fusion Eng. Des. (to be published).

[6] S. Ishiyama, Y. Muto, Y. Kato, S. Nishio, T. Hayashi and Y. Nomoto, Prog. Nucl. Energy **50**, No.12-6, 325 (2008).

[7] S. Ishiyama, T. Tanaka, A. Sagara and H. Chikaraishi, Fusion Sci. Technol., DOI: https://doi.org/10.1080/15361055.2019.1658046 (2019).

[8] C.W. White, N.T. Weiland, W.W. Shelton and T.R. Shultz, The 6th International Supercritical CO_2 Power Cycles Symposium March 27 - 29, 2018, Pittsburgh, Pennsylvania, 135.

[9] M. Penkuhn and G. Tsatsaronis, The 6th International Supercritical CO_2 Power Cycles Symposium March 27 - 29, 2018, Pittsburgh, Pennsylvania, 052.

[10] P. Sharan, T. Craig and T. Neises, The 6th International Supercritical CO_2 Power Cycles Symposium March 27 - 29, 2018, Pittsburgh, Pennsylvania, 187.

[11] J. Cho, H. Shin, H. Ra, C. Roh et al., The 6th International Supercritical CO_2 Power Cycles Symposium March 27 - 29, 2018, Pittsburgh, Pennsylvania, 102.

[12] A. Chaudhary, Y. Trivedi, A. Mulchand, H. Chauhan, P. Dave et al., The 6rh International Supercritical CO_2 Power Cycles Symposium March 27 - 29, 2018, Pittsburgh, Pennsylvania, 051.

[13] C. Spadacini, E. Pesatori, L. Centemeri, N. Lazzarin et al., The 6th International Supercritical CO_2 Power Cycles Symposium March 27 - 29, 2018, Pittsburgh, Pennsylvania, 113.

[14] J. Schmitt, J. Nielson and N. Poerner, The 6th International Supercritical CO_2 Power Cycles Symposium March 27 - 29, 2018, Pittsburgh, Pennsylvania, 090.

[15] M. Enoeda, Y. Kosaku, T. Hatano et al., Design and technology development of solid breeder blanket cooled by supercritical water in Japan, J. Nucl. Fusion **43**, 1837e1844 (2003).

[16] T. Ishizuka, Y. Kato, et al., Thermal-hydraulic characteristics of printed circuit heat exchanger in super critical CO2 loop. In: Proceedings of NURETH-11, October 2e6, Avignon, France, 2005.

[17] Y. Kato, T. Nitawaki and Y. Muto, Medium temperature carbon dioxide gas turbine reactor, Nucl. Eng. Des. **230**, 195 (2004).

[18] Y. Kato, Y. Muto, T. Ishizuka and M. Mito, Design of recuperator for the supercritical CO_2 gas turbine fast reactor. In: Proceedings of ICAPP05, 5196, May 15e19, Seoul, Korea, 2005.

[19] IHI technical report, Vol.47, No3, 102-108 (2007-9) (in Japanese).

[20] J. Miyazawa, T. Goto, H. Tamura et al., Plasma Fusion Res. **14**, 1405163 (2016).

[21] J. Miyazawa, T. Goto, H. Tamura et al., 30th SOFT (2018, Sicily), P1, 003.

[22] J. Miyazawa, T. Goto, H. Tamura et al., The strategy toward realization of helical fusion reactor, FFHR-c1, Fusion Eng. Des. **146**, lpart B, 2233 (September 2019).

[23] https://www.nist.gov

[24] D.S. Aziaka, E.O. Osigwe and B.T. Lebel-Alawa, Structural and Conceptual Design Analysis of an Axial Compressor for a 100 MW Industrial Gas Turbine (IND100). World Journal of Mechanics **4**, 332 (2014).

[25] N.A. Cumpsty, *Compressor Aerodynamics, 5th Edition*, Longman (London, 1999).

[26] Reynolds Number | Definition, Calculation & Examples | nuclear-power.net (nuclear-power.net).

[27] https://en.Wikipedia.org/wiki/flow_coefficient

[28] D.S. Aziaki, E.O. Osigwe and B.T. Lebel-Alawa, Structural and conceptual design analysis of an axial compressor for a 100 MW industrial gas turbine (IND100), World Journal of Mechanics **4**, 332 (2014).